International Journal of Engineering Technology and Scientific Innovation

ISSN: 2456-1851

Volume: 05, Issue: 04 "July-August 2020"

DESIGN AND SIMULATION OF PERFORMANCE OF A GAS TURBINE COMPRESSOR RUNNING ON SYNGAS

Liz Maina, Dr. (Eng.) H. Ndiritu, Dr. B. Gathitu

Department of mechanical engineering, JKUAT University, Kenya

DOI: 10.46609/IJETSI.2020.v05i04.003 **URL:** https://doi.org/10.46609/IJETSI.2020.v05i04.003

ABSTRACT

There is an increase in demand for electricity globally. Kenya relies heavily on hydropower as the main source of electricity. Gas turbines running on syngas are being used to generate electricity. This is because syngas is a renewable source of energy. As of 1999, General Electric (GE) had twelve gas turbines in operation using syngas in Delaware, and Singapore. Though gas turbines using syngas are in use, there is little literature showing the performance of the compressors in the gas turbines and specifically centrifugal compressors. This research focused on the performance of a centrifugal compressor running on syngas and compares its performance with that running on air. The centrifugal compressor designed was unshrouded with 15 main blades at a back-sweep angle of 45^0 and a vaneless diffuser. An initial rotational speed of 22,000 RPM was input with a mass flowrate 0.167kg/s for air. This research can be applied to industries working with syngas gas turbines for power generation, and compressing syngas for domestic use. Research can be further streamlined to focus on using syngas as a fuel for automobiles.

Keywords: Integrated Gasification Combined Cycle, Analysis system

1. INTRODUCTION

Energy demand has grown rapidly because of development of countries and the improvement of living standards. This has led to the increase in use of coal by 68%, natural gas by 62%, oil by 25%, hydropower by 21%, and nuclear energy by 13% over the last two decades.

Electricity is the world's fastest-growing form of end-use energy consumption. Fossil fuels and coal have been used to produce electricity in most countries.

In KenGen's 2017 annual report, thermal energy accounted for 16% of the electricity capacity mix. This translates to over 250MW of installed capacity. Thermal energy is from both diesel

ISSN: 2456-1851

Volume: 05, Issue: 04 "July-August 2020"

engines and gas turbines. The diesel engines run on HFO while the gas turbines run on kerosene. The gas turbines have an installed capacity of 60MW and they have been installed in Embakasi and Muhoroni.

Implementation of coal projects in the electric power industry is hampered by negative environmental and health impact of run-of-mine coal combustion. When coal is burned in its raw form, it emits green-house gases like carbon dioxide (CO_2), carbon monoxide (CO), methane (CH_4), mercury and other toxic gases.

The use of syngas energy is one way to generate clean energy. Syngas fuels are obtained from coal, biomass or solid waste gasification processes. Gasification involves burning materials that have carbon in limited supply of oxygen. A feature of syngas is that, unlike the raw fuels it is derived from, it can be used in gas turbine systems.

The main objective was to develop and simulate performance of gas turbine compressors running on syngas derived from coal.

2. LITERATURE REVIEW

A simple gas turbine comprises of a compressor, combustor, and a turbine. The compressor increases the pressure of the operating fluid. The fluid then moves to the combustor where it is ignited, and then to the turbine where it is expanded and its energy is used to turn the turbine. Centrifugal compressors comprise of impeller blades, hub, shroud, diffuser, and inlet guide vanes.

The operating range and performance parameters governing the compressor characteristics, i.e. pressure ratio, mass flow rate, and efficiency, and are commonly described in a compressor specific operation map. Centrifugal compressors can attain higher pressure ratios at one stage than axial compressors, and can be used where high speeds are required. Flow inside centrifugal compressors shows complex three-dimensional features due to compact structure, radial blade profiles, and strong adverse pressure gradients, especially for high pressure-ratio compressors.

2.1 Flow Instabilities in Centrifugal Compressor

Surge is defined as an unstable condition which causes flow reversal and pressure fluctuations. It occurs when there is resistance to flow. Surge is basically a phenomenon of air stalling with partial flow reversal in the compressor. Kurz et al. [27] defined choke as a blockage experienced in the blade flow passages that occur during high flowrates. Surge and stall negatively affect the efficiency of the compressor. The effects of surge include exponential temperature increase,

ISSN: 2456-1851

Volume: 05, Issue: 04 "July-August 2020"

process instability, potential machine trip, process shutdown and machine damage.

Surge occurrence is affected by how complex the compression system is such as increase in impeller blades. Few surge cycles can be tolerated by centrifugal compressors as long as the impulse or energy of the reversed flow is small in relation to the mass of the compressor rotating assembly.

Bernhard et al. analyzed flow through a centrifugal compressor with a ported shroud and a vaneless diffuser. The mass flowrate was reduced gradually from a stable operation range to unstable operating range. Modal decomposition was used to characterise the flow leading to surge. The centrifugal compressor used had 10 main blades with no splitter blades and the blades were at a backsweep angle of 25^0. Zheng et al. investigated the flow instabilities in a centrifugal compressor with a vaneless diffuser. High-response pressure probes were used to capture the change in conditions within the compressor at high speeds. At speeds of less than 70% of the maximum speed and at low mass flowrates, stall was induced at the impeller inlet. When the flowrate was further reduced, the stall became surge and this surge extended to the diffuser. It was also observed that at 70% of the maximum speed, mild surge emerged. Zheng et al. concluded that at different operating conditions, different surge patterns occur [24].

The medium used was air, there is therefore a gap to use syngas as a medium and determine the surge patterns that will result.

Kurz et al. [27] simulated flow through a multistage centrifugal compressor. The aim was to investigate the compressor's operation during choke and resultant axial thrust loading. The compressor had 19 main blades. He found out that vaneless diffuser has no effect when a compressor is operating in choke. From his analysis, as inlet flow coefficient increased, the thrust bearing temperature also increased. His final conclusion was that operating a centrifugal compressor in choke was not a problem if the balance piston provides adequate thrust and if the impeller blade was strong enough to withstand the alternating stresses.

2.2 Working Fluids in Gas Turbines

Syngas is composed of fuels such as H_2, CO, and CH_4 and inert diluents such as N_2 and CO_2. These diluents influence the ignition of syngas by reducing the temperature of the air/fuel mixture heading to the spark and hence reducing the initial flame kernel.

Filippis et al. used olive husks in an industrial scale plant. The syngas produced was fed to an internal combustion engine. Their aim was to remove tar produced during gasification using a second reactor. They were able to remove more than 50% of the tar produced. With the removal

ISSN: 2456-1851

Volume: 05, Issue: 04 "July-August 2020"

of tar, they proved that it is possible to remove impurities earlier on in the gasification process in order to reduce the energy needed for purification. The syngas produced was fed to an internal combustion engine which generated 60kWe and an efficiency of 25% was achieved. Suhui et al. [38] investigated the behavior of syngas in spark ignition using gas turbine start up conditions, and the effects of the syngas fuel composition and air flow on ignition performance. They discovered that syngas has better ignition performance as compared to natural gas though one of the hindrance of using syngas in gas turbine is its change in composition and heating value.

3. METHODOLOGY

3.1 Modeling of the Centrifugal Compressor

In this study, focus was on the impeller since it imparts the fluid with momentum and it is also where instabilities like surge and stall occur. The centrifugal compressor was modeled using vista CCD which is an inbuilt component system in Ansys 19.0.

3.2 Geometric Modeling

The computational space was modeled as a vaneless diffuser consisting of an unshrouded impeller having 15 blades. This was based on the criteria from previous studies showing an increase in efficiency for blade number between 12 and 15 and the optimum blade number was 15. Further the selection of an unshrouded impeller was based on the criteria that unshrouded impellers have higher tip speeds which result in an increase of volume flow and head. Micro-gas turbines have the advantages of being light weight, having greater efficiency, low capital cost, and a small number of moving parts.

3.3 BladeGen Design

Compressor data was transferred from Vista CCD to BladeGen. This is because data cannot be transferred directly from Vista CCD to mesh in Ansys. Initial blade set-up was defined and this included the number of blades. Figure below shows the meridional view of the centrifugal compressor. The blade shape was defined by the number of layers and in this case, there were 4 layers. This number was generated automatically in BladeGen.

ISSN: 2456-1851

Volume: 05, Issue: 04 "July-August 2020"

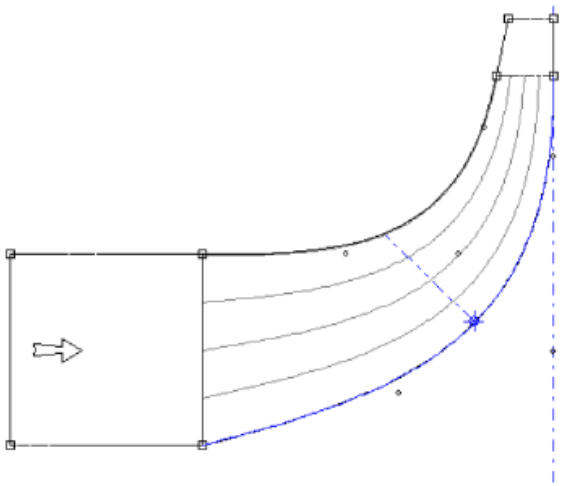

Figure 1: Meridional view

With the data from Vista CCD, the blade and layer parameters were generated automatically in BladeGen.

3.4 Mesh Generation

It was necessary to generate a mesh that would facilitate flow simulation. This entailed discretization of model into cells and nodes. For the regions having severe flow gradients, it was essential to refine the mesh.

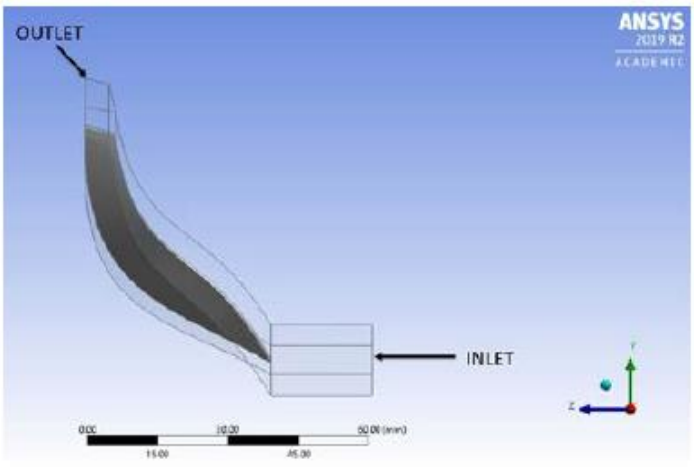

Figure 2: Fluid Flow Zone before Meshing

ISSN: 2456-1851

Volume: 05, Issue: 04 "July-August 2020"

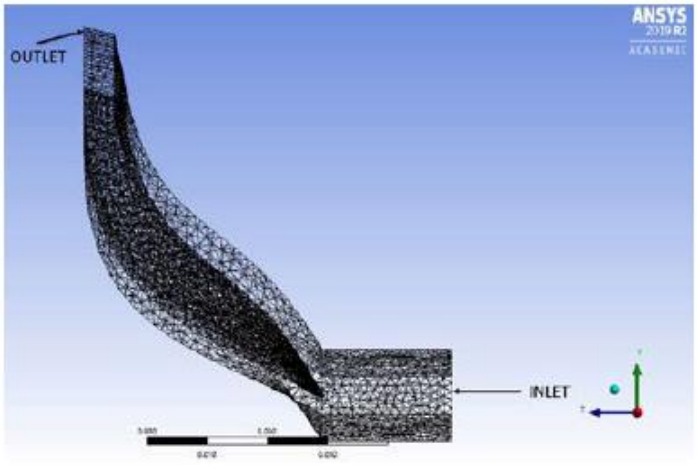

Figure 3: Fluid Flow Zone after Meshing

The type of mesh selected was tetrahedron because they have high level of flexibility control of grid parameters such as cell shape and size, and they are best for complex geometries.

3.5 Governing Equations

Flow conservation equations were solved to simulate the behavior of the fluid across the compressor. These flow equations included mass, momentum, species conservation and energy equations and they were expressed in Cartesian coordinate system.

a. Mass conservation equation

$$\frac{\partial \rho}{\partial t} + \nabla.(\rho V) = \frac{\partial \rho}{\partial t} + \frac{\partial \rho u}{\partial x} + \frac{\partial \rho v}{\partial y} + \frac{\partial \rho w}{\partial z} = 0$$

b. Momentum conservation equation

ISSN: 2456-1851

Volume: 05, Issue: 04 "July-August 2020"

$$\rho\frac{Du}{Dt} = \rho f_x - \frac{\partial P}{\partial x} + \frac{\partial}{\partial x}\left[\mu\left(-{}^2/_3\,\nabla.V + 2\frac{\partial u}{\partial x}\right)\right] + \frac{\partial}{\partial y}\left[\mu\left(\frac{\partial v}{\partial x} + \frac{\partial u}{\partial y}\right)\right] + \frac{\partial}{\partial z}\left[\mu\left(\frac{\partial w}{\partial x} + \frac{\partial u}{\partial z}\right)\right]$$

$$\rho\frac{Dv}{Dt} = \rho f_y - \frac{\partial P}{\partial y} + \frac{\partial}{\partial y}\left[\mu\left(-{}^2/_3\,\nabla.V + 2\frac{\partial v}{\partial y}\right)\right] + \frac{\partial}{\partial x}\left[\mu\left(\frac{\partial v}{\partial x} + \frac{\partial u}{\partial y}\right)\right] + \frac{\partial}{\partial z}\left[\mu\left(\frac{\partial w}{\partial y} + \frac{\partial v}{\partial z}\right)\right]$$

$$\rho\frac{Dw}{Dt} = \rho f_z - \frac{\partial P}{\partial z} + \frac{\partial}{\partial z}\left[\mu\left(-{}^2/_3\,\nabla.V + 2\frac{\partial w}{\partial z}\right)\right] + \frac{\partial}{\partial x}\left[\mu\left(\frac{\partial w}{\partial x} + \frac{\partial u}{\partial z}\right)\right] + \frac{\partial}{\partial y}\left[\mu\left(\frac{\partial w}{\partial y} + \frac{\partial v}{\partial z}\right)\right]$$

c. Energy conservation equation

$$\rho C\frac{DT}{Dt} = \rho C\left(\frac{\partial T}{\partial t} + V.\nabla T\right)$$

3.6. SST Turbulence Model

This model was selected since it integrates features of both $k-\omega$ and $k-\epsilon$ model.

Modeled equation for turbulent kinetic energy k was:

ISSN: 2456-1851

Volume: 05, Issue: 04 "July-August 2020"

$$\frac{\partial(\rho k)}{\partial t} + \frac{\partial(\rho u_j k)}{\partial x_j} = P - \beta\rho\omega k + \frac{\partial}{\partial x_j}[(\mu + \sigma_k \mu_t)\frac{\partial k}{\partial x_j}]$$

The boundary conditions were as shown below:

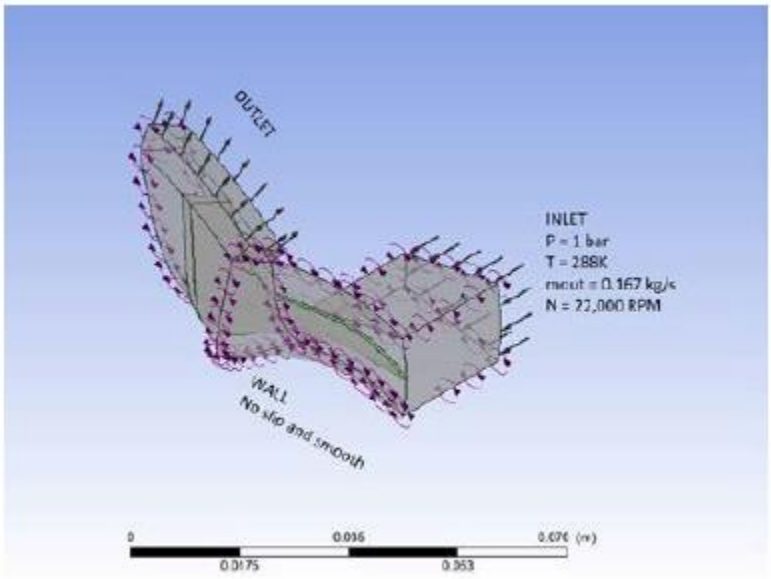

Figure 4: Boundary Conditions

4. RESULTS AND DISCUSSION

4.1 Pressure Variations

4.1.1 Air

The figure below shows the pressure variation of air at a rotational speed of 22,000 RPM and a mass flowrate of 0.167kg/s. As the air flows through the compressors, its pressure increases from 1 bar to around 1.4 bar. There is a region of low pressure on the suction side as the flow changes

ISSN: 2456-1851

Volume: 05, Issue: 04 "July-August 2020"

direction.

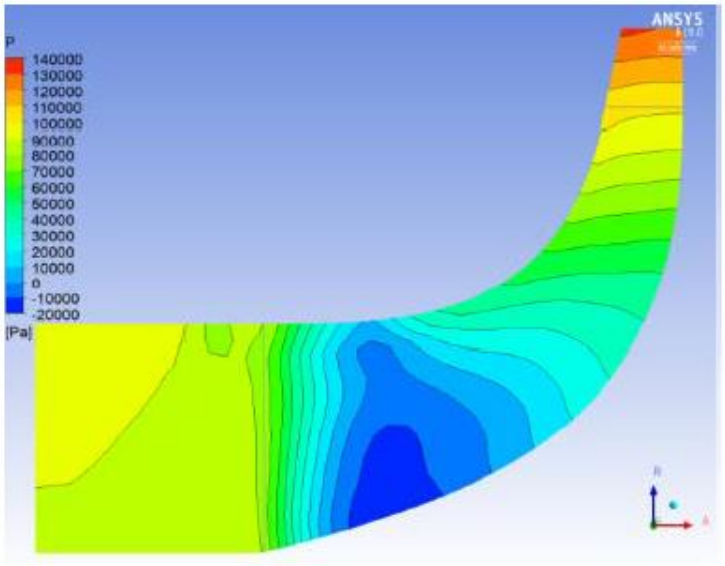

Figure 5: Pressure Contour at 22000 RPM

As the rotational speed increased, the pressure contours changes as shown below.

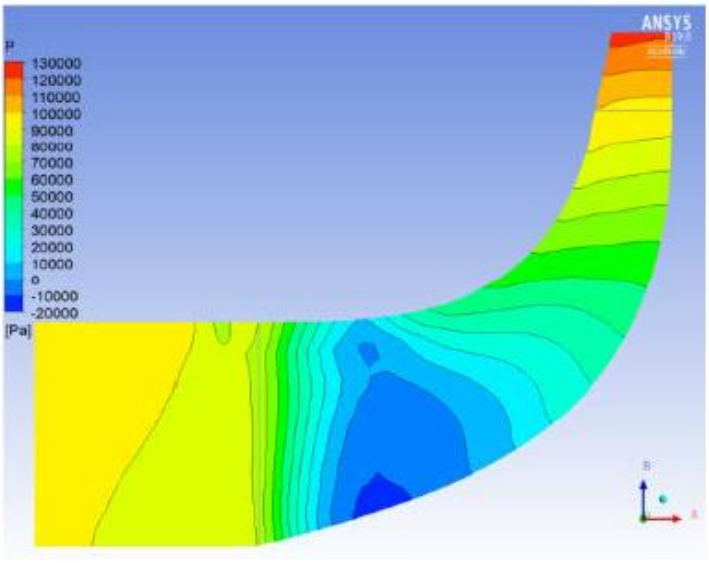

Figure 6: Pressure Contour at 21000 RPM

ISSN: 2456-1851

Volume: 05, Issue: 04 "July-August 2020"

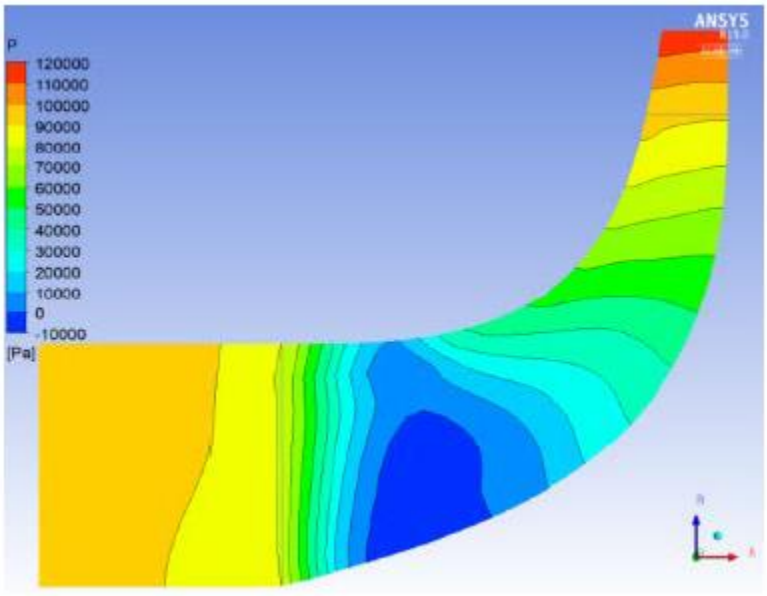

Figure 7: Pressure Contour at 20000 RPM

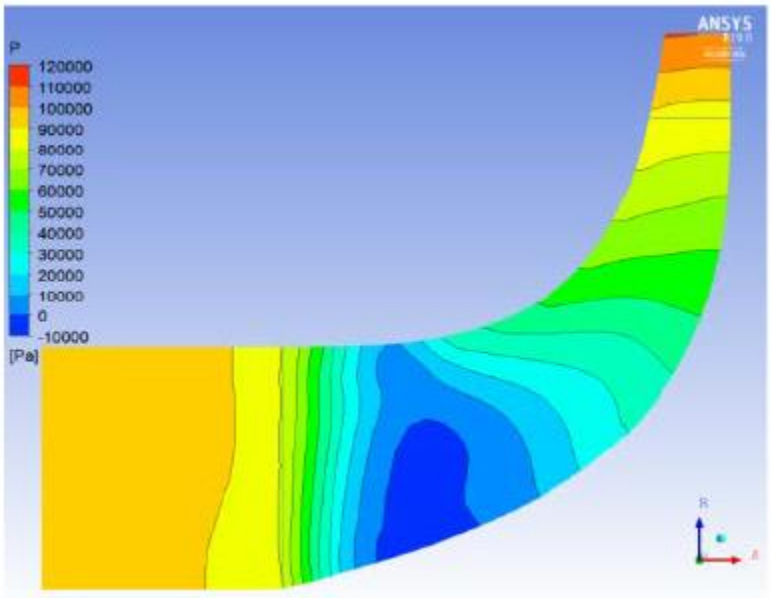

Figure 8: Pressure Contour at 19000 RPM

ISSN: 2456-1851

Volume: 05, Issue: 04 "July-August 2020"

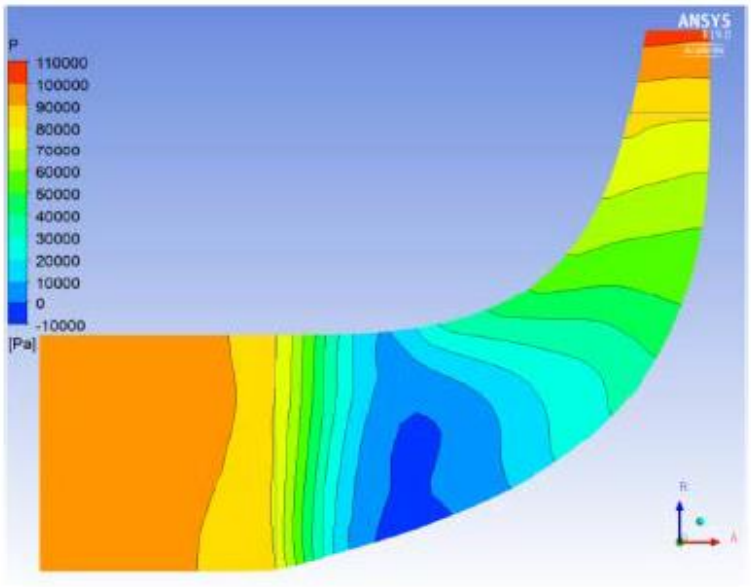

Figure 9: Pressure Contour at 18000 RPM

4.1.2 Syngas

The behavior of syngas differed from that of air. This is because syngas has a lower molecular weight of 7-10g/mol which is 1/3 of that of air.

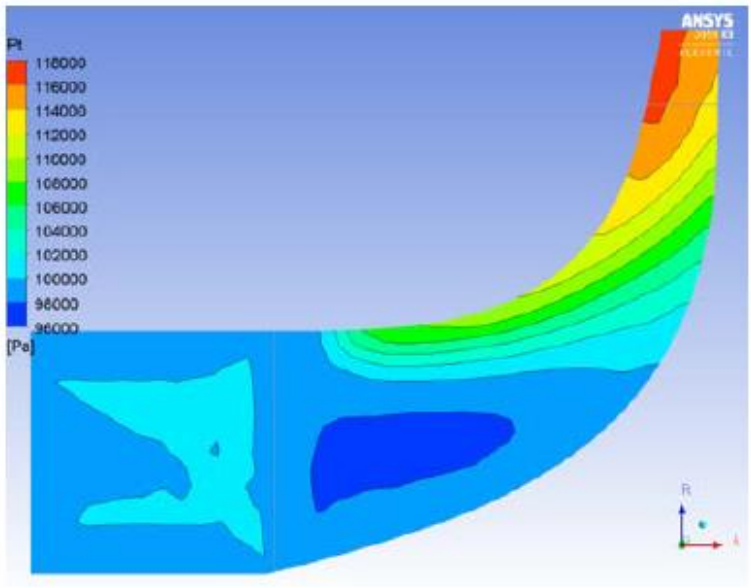

Figure 10: Syngas Pressure Contour at 22000 RPM

ISSN: 2456-1851

Volume: 05, Issue: 04 "July-August 2020"

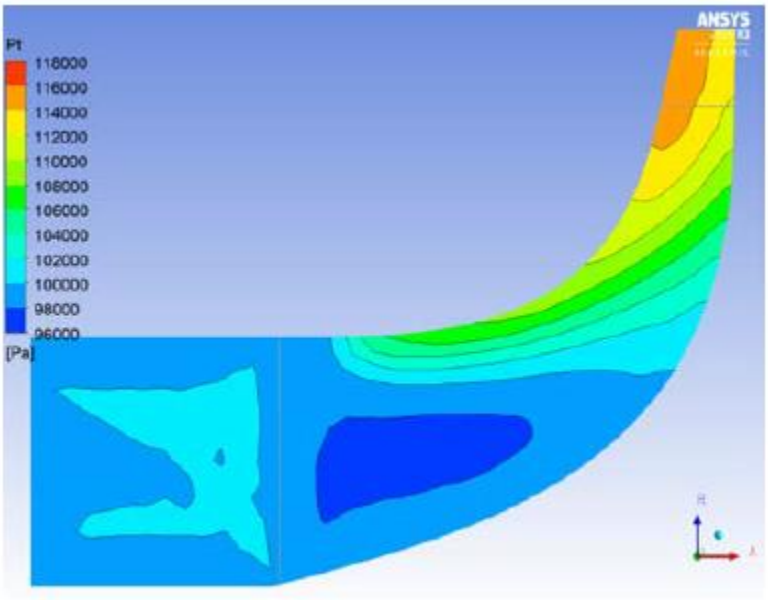

Figure 11: Syngas Pressure Contour at 21000 RPM

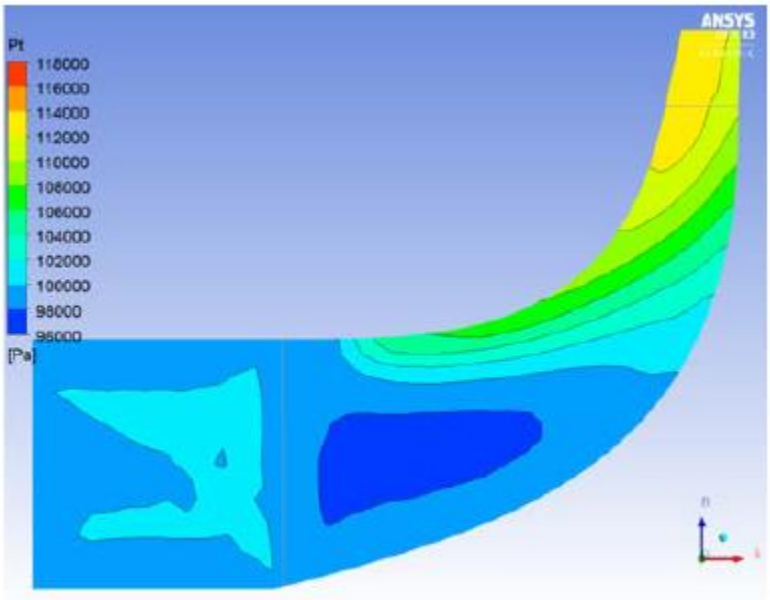

Figure 12: Syngas Pressure Contour at 20000 RPM

ISSN: 2456-1851

Volume: 05, Issue: 04 "July-August 2020"

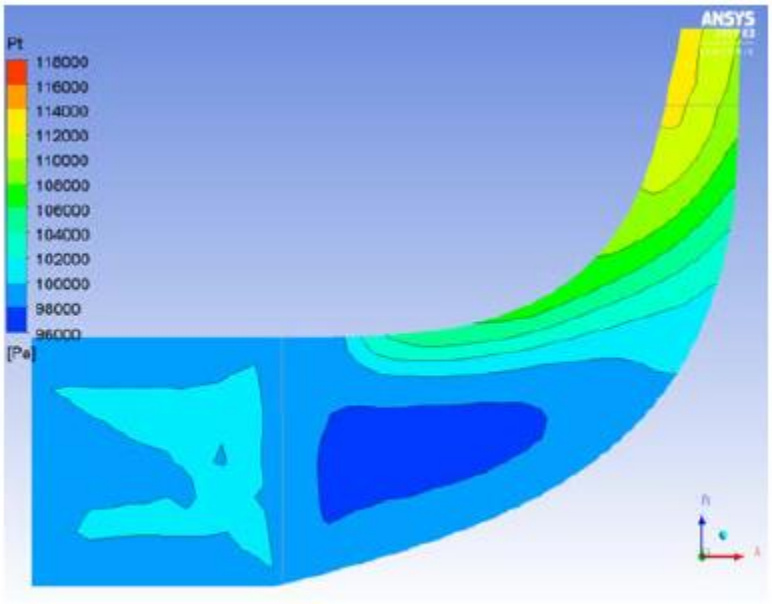

Figure 13: Syngas Pressure Contour at 19000 RPM

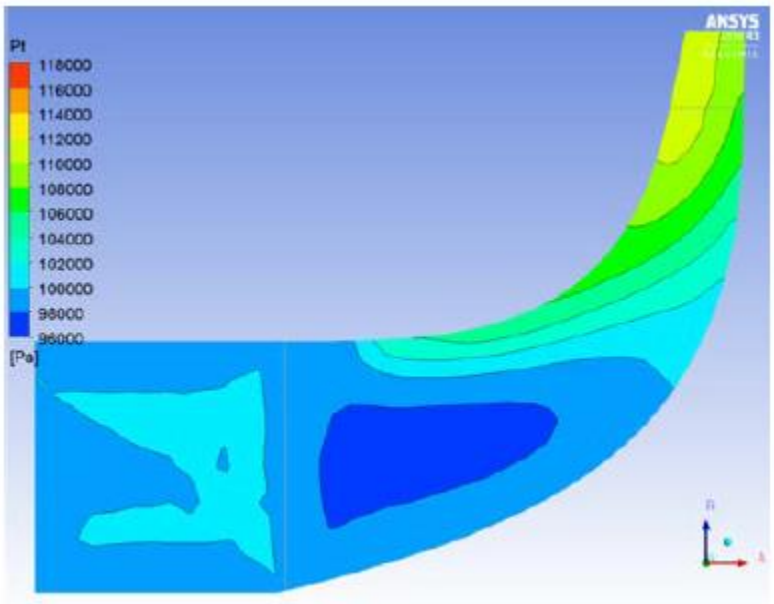

Figure 14: Syngas Pressure Contour at 18000 RPM

ISSN: 2456-1851

Volume: 05, Issue: 04 "July-August 2020"

4.2 Velocity Variation

4.2.1. Air

Velocity flow through the compressor varied from shroud to hub along the blades. The figures below show velocity changes at streamwise location of 20%, 50% and 80% span.

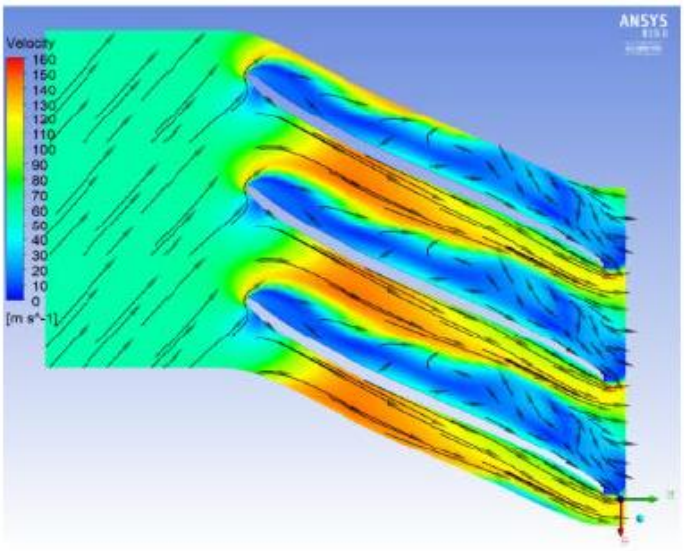

Figure 15: Velocity Vectors at 20% Span

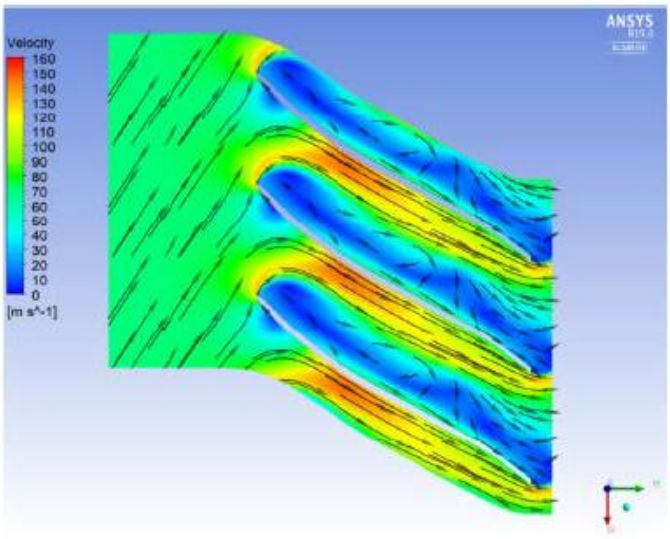

Figure 16: Velocity Vectors at 50% Span

ISSN: 2456-1851

Volume: 05, Issue: 04 "July-August 2020"

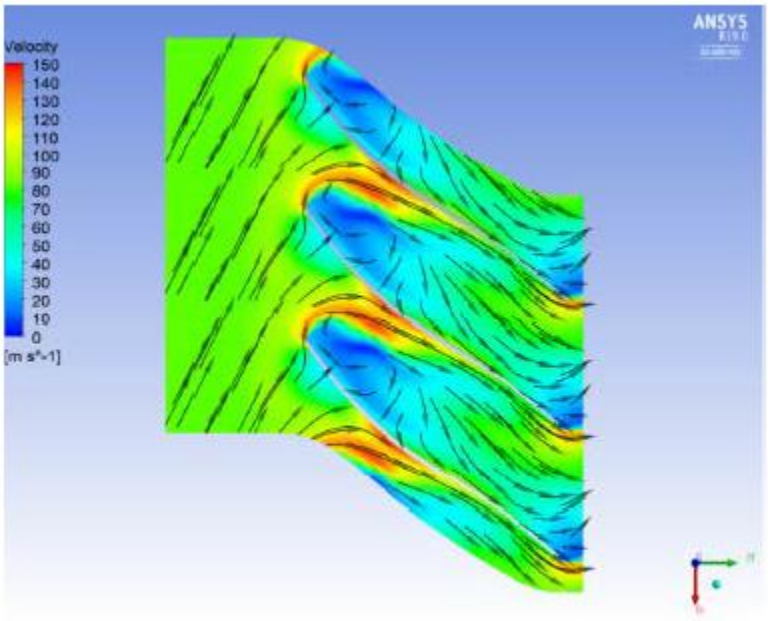

Figure 17: Velocity Vectors at 80% Span

There is a region of low velocity of 20m/s at the pressure side of the impeller blades. In this region, recirculation of air occurs and this is the choking area. As the streamwise location moves to 50% span, the low velocity region reduces. At 80% span, it can be seen that the low velocity region moves upstream. There is a slight increase in velocity at the trailing edge of the impeller blades. The highest velocity attained is 150m/s.

4.2.2. Syngas

Flow of syngas through the impeller was quite different from that of air. This is mainly due to the low molecular weight of syngas coupled with low mass flowrate through the compressor at high speeds. There was minimal recirculation at 80% span.

ISSN: 2456-1851

Volume: 05, Issue: 04 "July-August 2020"

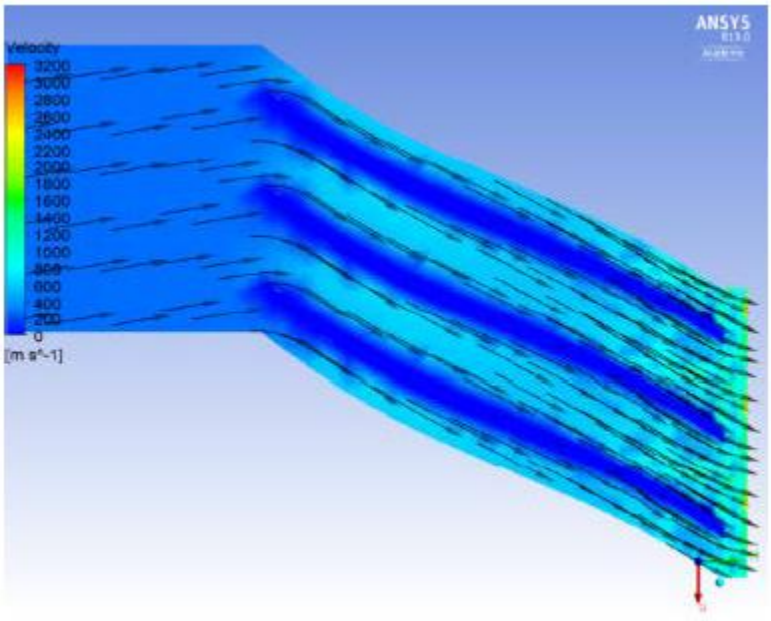

Figure 18: Syngas Velocity Vectors at 20% Span

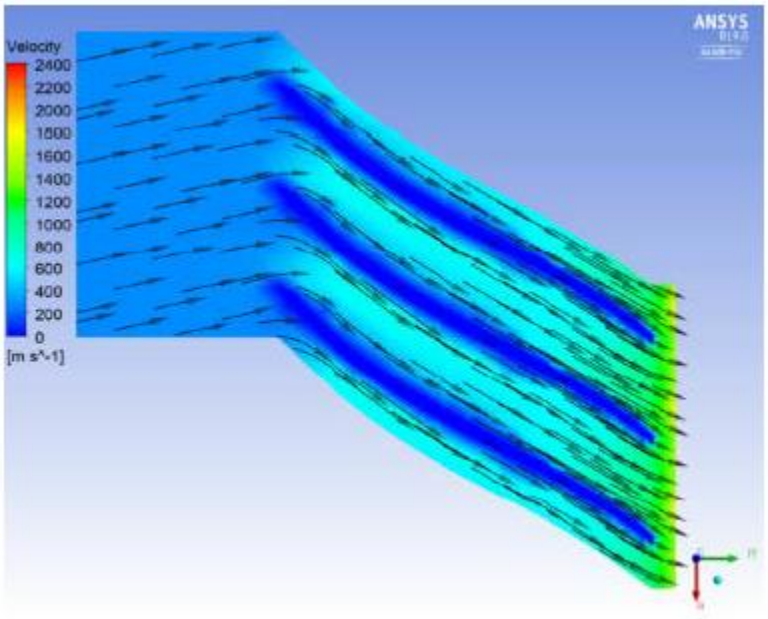

Figure 19: Syngas Velocity Vectors at 50% Span

ISSN: 2456-1851

Volume: 05, Issue: 04 "July-August 2020"

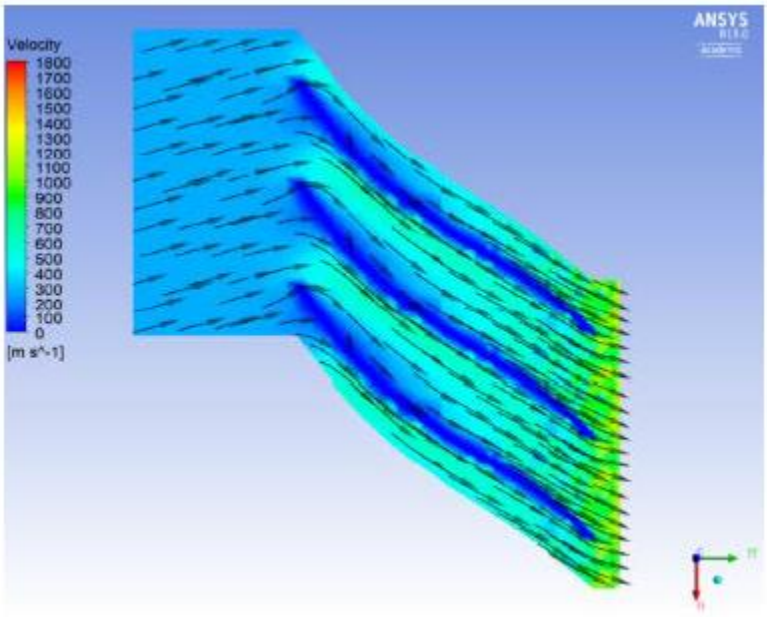

Figure 20: Syngas Velocity Vectors at 80% Span

4.3 Mach Number Variation

4.3.1. Air

The figures below show the change in relative Mach number at a rotational speed of 22000RPM. It can be seen that the Mach number is higher on the suction side than on the pressure side of the impeller blades. The regions of low Mach number reduce as you move from the shroud to the hub.

ISSN: 2456-1851

Volume: 05, Issue: 04 "July-August 2020"

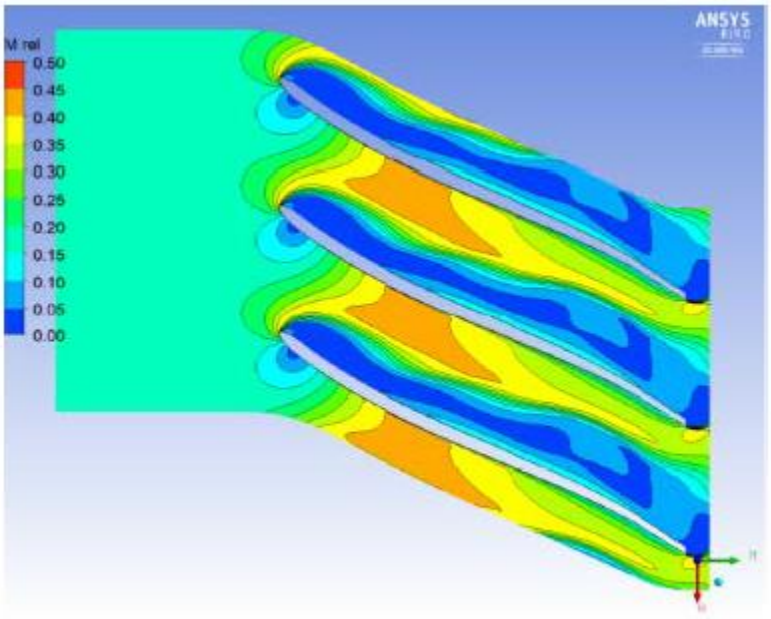

Figure 21: Relative Mach Number at 20% Span

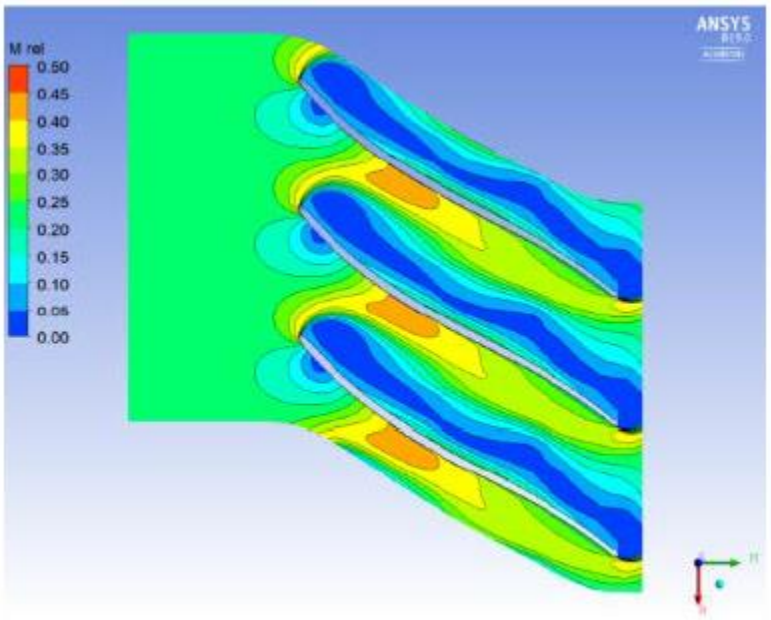

Figure 22: Relative Mach Number at 50% Span

ISSN: 2456-1851

Volume: 05, Issue: 04 "July-August 2020"

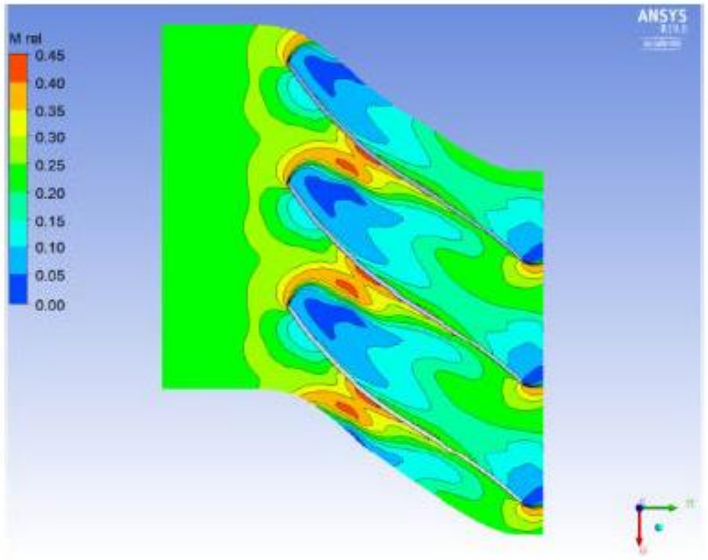

Figure 23: Relative Mach Number at 80% Span

4.3.2.Syngas

For syngas, low Mach number was experienced throughout the compressor. There was a slight increase of Mach number towards the hub, at 80% span.

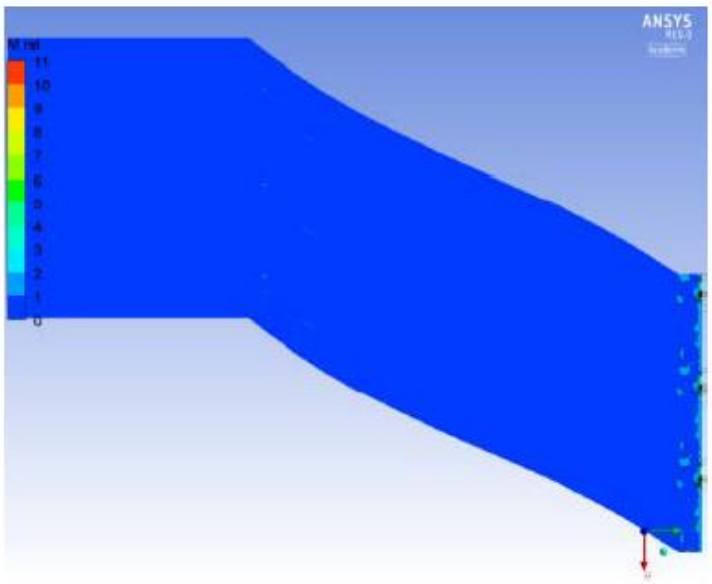

Figure 24: Relative Mach Number for Syngas at 20% Span

ISSN: 2456-1851

Volume: 05, Issue: 04 "July-August 2020"

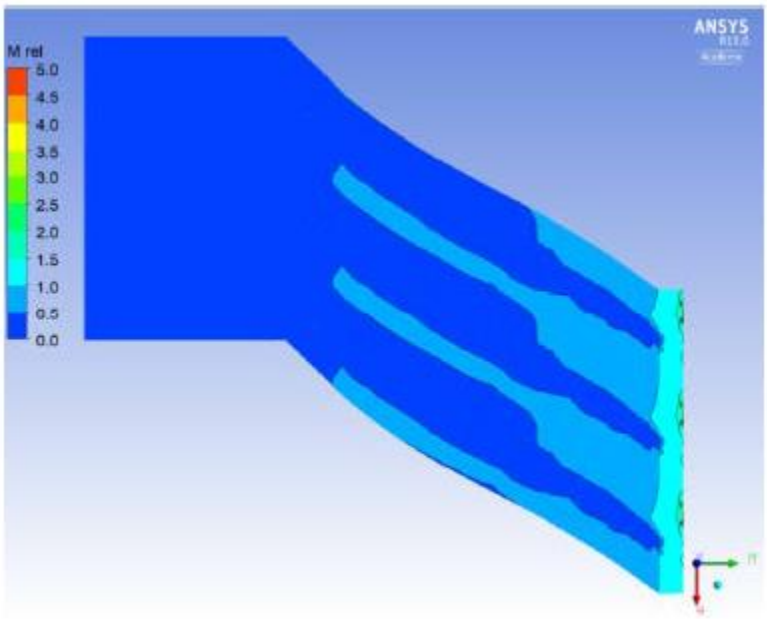

Figure 25: Relative Mach Number for Syngas at 50% Span

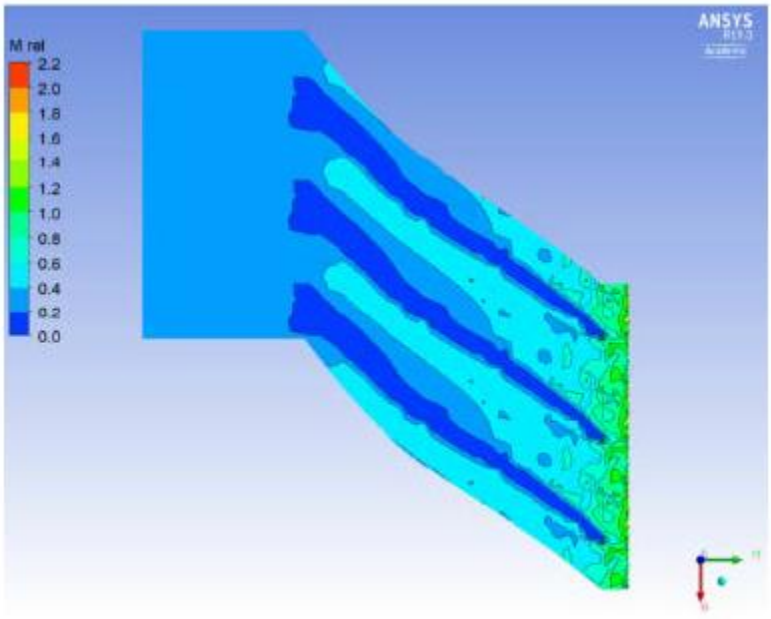

Figure 26: Relative Mach Number for Syngas at 80% Span

ISSN: 2456-1851

Volume: 05, Issue: 04 "July-August 2020"

4.4 Efficiencies

The figures below show the isentropic efficiencies for air and syngas. As the flowrate increases at a constant rotational speed, the efficiency reduces. This is expected since the same speed is required to do more work therefore the efficiency will be low. The efficiency for syngas is much lower than that of air.

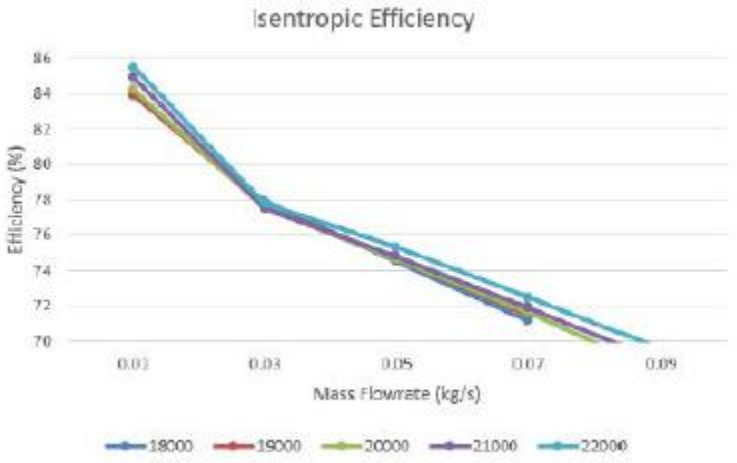

Figure 27: Isentropic Efficiency of Air

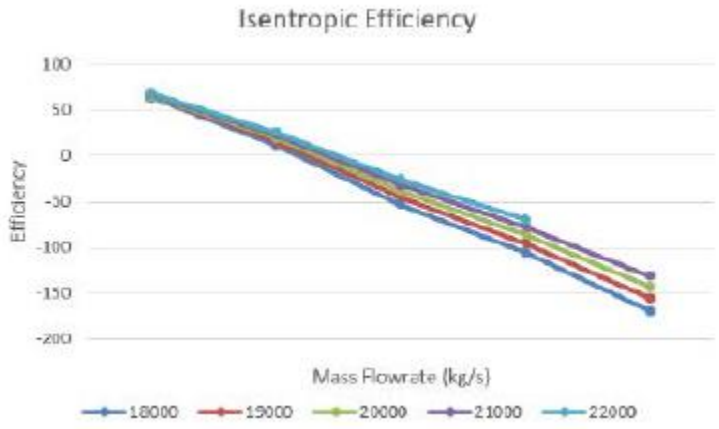

Figure 28: Isentropic Efficiency of Syngas

ISSN: 2456-1851

Volume: 05, Issue: 04 "July-August 2020"

5. CONCLUSION AND RECOMMENDATIONS

This paper shows the difference in using air and syngas in a centrifugal compressor. Air and syngas were compressed in a centrifugal compressor running at a speed of 22000RPM. Rotational speed and mass flowrate were varied and the results were presented. Syngas has shown more stability across the compressor as compared to air. This is because of the low areas of recirculation experienced.

Further analysis can be done on the different syngas ratios to determine the optimum H_2/CO ratio. The compressor stages can also be increased and the changes in pressure ratio investigated.

REFERENCES

1. Zemp, “CFD Investigation on Inlet Flow Distortion in a Centrifugal Compressor" *Master's thesis, Swiss Federal Institute of Technology,* ETH, Zurich Turbomachinery Laboratory, 2006/2007.
2. “World Energy Trilemma Index" 2018.
3. R. Brdar “GE IGCC Technology and Experience with Advanced Gas Turbines," Tech. Report, General Electric (GE).
4. D. Burnes “Performance Degradation Effects in Modern Industrial Gas Turbines" *In- Proceedings of Zurich 2018 Global Power and Propulsion Forum, 2018.*
5. S. Oyedepo “Thermodynamic Analysis of a Gas Turbine Power Plant Modeled with an Evaporative Cooler" *International Journal of Thermodynamics (IJoT), vol. 17 pp. 14- 20, 2014.*
6. I. J. Day “Stall, Surge, and 75 Years of Research" *Journal of Turbomachinery, ASME, vol. 138, 2016.*
7. R. Kurz “Operation of Centrifugal Compressors in Choke Conditions" *Proceedings of the Fortieth Turbomachinery Symposium, pp. 129- 136, 2011.*
8. Z. Xinqian “Experimental Investigation of Surge and Stall in a High-Speed Centrifugal Compressor" *Journal of Propulsion and Power, vol. 31, 2015.*
9. Semlitsch “Flow Phenomena Leading to Surge in a Centrifugal Compressor" *Elsevier, vol. 103, pp. 572-587, 2016.*
10. S. Noman “The Influence of Tip Clearance on Centrifugal Compressor Stage of a Turbocharger" *In- Proceedings of the 4th WSEAS International Conference on Fluid Mechanics and Aerodynamics, Elounda, Greece, 2006.*

